Geologica Acta, Vol.11, Nº 2, June 2013, 149-165
DOI: 10.1344/105.000001841
Available online at www.geologica-acta.com

geologica acta

The Case for UHP Conditions in the Cuaba Terrane, Río San Juan Metamorphic Complex, Dominican Republic

R.N. ABBOTT Jr.[1,*] **and G. DRAPER**[2]

[1] **Department of Geology, Appalachian State University**
Boone, NC, 28608 USA. E-mail: abbottrn@appstate.edu

[2] **Department of Earth Sciences, Florida International University**
Miami, FL, 33199 USA. E-mail: draper@fiu.edu

*Corresponding author

ABSTRACT

This paper is essentially a review of previously published data and interpretations for ultramafic and eclogitic rocks from the Cuaba terrane in northern Dominican Republic. Ultrahigh pressure (UHP) conditions are indicated for the Cuaba terrane on the basis of phase relationships in garnet-bearing ultramafic rock. Dikes and orthocumulate textures indicate a magmatic origin. Mineral assemblages define a line of descent controlled by fractional crystallization. The original estimate of the magmatic conditions (P>3.4GPa, T>1550°C) was inferred previously from available high-P melting experiments in the CMAS system and high-P experimental determination of the sapphirine-out reaction in the MAS system. Revised estimates of magmatic conditions (P>3.2GPa, T>1500°C) take into account the influence of other components, especially Fe. We propose an origin in the mantle-wedge above a subduction zone. The rock was delivered to the subduction zone by forced convection in the mantle wedge (corner-flow), coupled with erosion of the hanging wall. Thermobarometry indicates >850°C and >3.4GPa when the ultramafic rock was incorporated into eclogite (deep-subducted oceanic crust).

Evidence for UHP conditions in the retrograded eclogite is not obvious. Two types of symplectic intergrowths, plagioclase + clinopyroxene (Sym-I) and plagioclase + epidote (Sym-II), are interpreted as the products of the decomposition of two types of omphacite, Omp-I and Omp-II. Theoretically, Omp-II formed as the result of a retrograde reaction of the form, Omp-II + coesite = Omp-I + kyanite + /- garnet, according to which the maximum pressure for Omp-II is between ~2.8GPa (~850°C) and ~4.2GPa (~950°C), consistent with subsolidus conditions for the garnet-bearing ultramafic rocks. For eclogite, the highest-pressure mineral assemblage would have been Omp-I + kyanite + garnet + coesite.

KEYWORDS | **Ultra high pressure. Garnet-bearing ultramafic rock. Eclogite. Dominican Republic.**

INTRODUCTION

Worldwide there are fewer than thirty coesite- or diamond-bearing ultra high pressure (UHP) terranes (Carswell and Campagnoni, 2003a; Liou *et al*., 2006), and a handful of terranes proposed to be UHP on the basis of evidence other than the signature presence of coesite or diamond. Most of the work on signature UHP terranes features locations in eastern China, the Alps, Norway, and Kazakhstan (*e.g*., Carswell and Campagnoni, 2003b;

Hacker *et al*., 2006; Liou and Cloos, 2006). Such terranes are interesting because they record events at the very greatest depths for the most part in continent-continent collisional zones.

At the time of its discovery (Abbott and Draper, 1998; Abbott *et al*., 2001) the proposed UHP Cuaba terrane in the Dominican Republic was the second in the Americas. The first discovery was in the Seward Peninsula, Alaska (Till, 1981; Liebermann and Till, 1987). Today, there are two other UHP locations in the Americas, one in eastern Brazil (Parkinson *et al*., 2001) and the suggestion of an occurrence in the Canadian part of the North American Cordillera (MacKenzie *et al*., 2005), but only the Dominican site shows such an unusual inventory of ultramafic mineral assemblages.

The Dominican Cuaba terrane is especially interesting for a number of reasons. The terrane was delivered to the surface at an ocean-ocean convergent plate boundary, confounding mechanisms of uplift involving buoyancy (*e.g*., Gorczyk *et al*., 2007). One of the ultramafic rock types, garnet clinopyroxenite, contains the only orogenic occurrence of coexisting garnet + spinel + corundum in the form of sub mm-scale inclusions of corundum and spinel in garnet (Abbott *et al*., 2005, 2006b; Gazel *et al*., 2012). Otherwise, natural occurrences of coexisting Grt + Spl + Crn are known only from rare alkremite and corgaspinite xenoliths in kimberlite (de Hoog, 2012). Laboratory experiments (Ackermand *et al*., 1975) show that the combination (Grt + Spl + Crn) is only possible at very high pressures (Abbott *et al*., 2005, 2006b; Gazel *et al*., 2011). Finally, the ultramafic rock offers an unusually detailed glimpse into magmatic processes in the mantle.

The objectives of this contribution are to review the evidence for UHP conditions in the Cuaba terrane, compare the P-T paths for the ultramafic rock and retrograded eclogite, and to speculate on a tectonic model for assembling the terrane and delivering it to the surface.

Abbreviations for minerals and components follow Kretz (1983), as updated by Whitney and Evans (2010). Three abbreviations for pyroxene components are introduced here, for the lack of guidance in Kretz (1983) and Whitney and Evans (2010): Ca-ts stands for Ca tschermak component, $CaAl_2SiO_6$; Ca-esk stands for Ca-eskola component, $[]_{1/2}Ca_{1/2}AlSi_2O_6$ (Smyth, 1980); Al-buf stands for Al-buffonite component, $CaMg_{1/2}Ti_{1/2}AlSiO_6$ (Sack and Ghiorso, 1994). Abbreviations for minerals are capitalized, *e.g*., Di=Cpx with di>90%, or Ab=Pl with ab>90%; abbreviations for components of a mineral are not capitalized, *e.g*., di in Cpx, or ab in Pl.

GEOLOGIC SETTING

The Dominican Republic occupies the eastern two-thirds of the island of Hispaniola, near the northern edge of the Caribbean Plate (Fig. 1). The basement of Hispaniola, and basements of neighboring Jamaica, Puerto Rico and the southern part of Cuba, started to form in the Early Cretaceous as an intra-oceanic island arc, above a subduction zone. The polarity of the original subduction zone remains controversial. Early interpretations advocated a Mid-Cretaceous (120-100Ma) polarity reversal from NE-dipping to the present W- to SW-dipping configuration (Pindell and Barrett, 1990; Draper *et al*., 1996, Pindell and Kennan, 2001, 2009). In this scenario, subduction ceased on the Pacific side of the island arc complex, 120-100Ma, only to resume with reversed polarity on the Atlantic side of the complex (Pindell and Barrett, 1990; Draper *et al*., 1996, Pindell and Kennan, 2001, 2009). Current thinking advocates that a reversal in polarity, as it relates to the Greater Antilles, need not have taken place (Mann *et al*., 2007; Stanek *et al*., 2009; Hastie *et al*., 2010; Pindell *et al*., 2012). That is, the polarity has always been as it is today, W- to SW-dipping. Regardless of the controversy concerning the polarity of subduction, throughout the late Cretaceous until the Middle Eocene, the Atlantic lithosphere dipped W to SW beneath the E and NE edge of the Caribbean plate. From the Late Cretaceous to Mid-Eocene, the intra-oceanic island arc expanded through magmatism and other accretionary processes (Pindell and Barrett, 1990; Draper *et al*., 1996; Pindell *et al*., 2005). Beginning in the mid-Eocene and continuing to the present, the island arc system has been modified by E-W, left-lateral, transcurrent and transpressional tectonics (Draper *et al*., 1996; Mann *et al*., 1990, 2002; Jansma *et al*., 2000).

The Cordillera Septentrional forms the landscape north of the Septentrional fault in the Dominican Republic (Fig. 1). The WNW-ESE trending range consists of Upper Eocene to Lower Miocene siliciclastic and carbonate sedimentary rocks, underlain by a basement of metamorphic and igneous rocks (Eberle *et al*., 1982; Lewis and Draper, 1990). The basement is exposed in a number of stratigraphic windows, or "inliers" where the cover has been eroded away. The largest of these inliers brings to light the Río San Juan metamorphic complex (Eberle *et al*., 1982; Draper and Nagle, 1991). Escuder-Viruete *et al*. (2011) offer a detailed map of the Río San Juan metamorphic complex. Figure 1 shows the geology near the southern margin of the complex.

The Río San Juan metamorphic complex (Draper and Nagle, 1991, Escuder-Viruete *et al*., 2011) is divided into distinct northern and southern parts, which were juxtaposed by faulting, probably in the Paleogene (Draper and Nagle, 1991; Draper *et al*., 1994). The northern part of the inlier

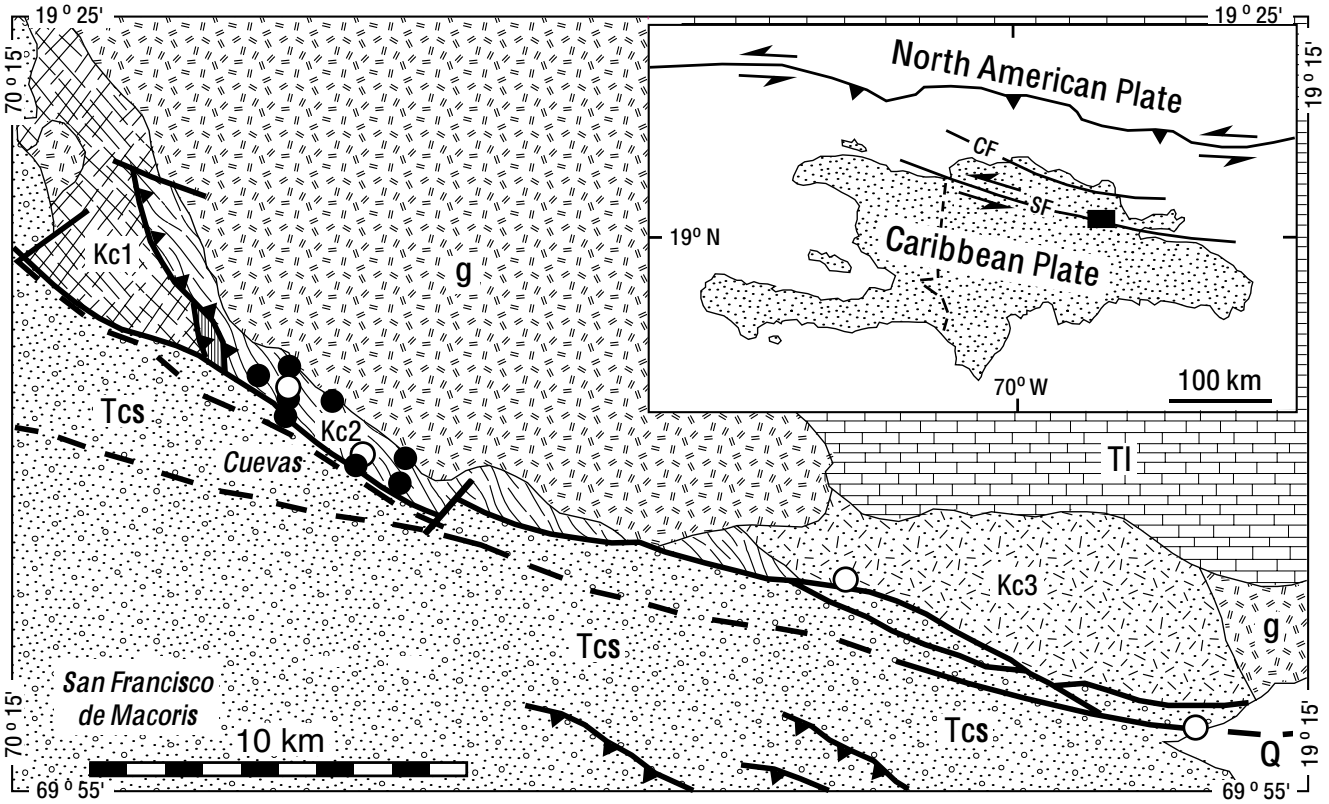

FIGURE 1 | Geology of the southern part of the Río San Juan metamorphic complex. The Island of Hispaniola is shown in the inset. The vertical dashed boundary separates Haiti (west) from the Dominican Republic (east). The Cordillera Septentrional forms the landscape immediately north of the Septentrional Fault (SF). Movement between the North American Plate and Caribbean Plate is accommodated by the Septentrional Fault (SF), Camu Fault (CF) and an offshore strongly oblique convergent zone (Jansma *et al.*, 2000; Mann *et al.*, 2002). The study area is marked by the filled rectangle. The geologic map shows the southern part of the Cretaceous Río San Juan metamorphic complex (re-mapped 2002-2005, cf. Draper and Nagle, 1991). The Cuaba terrane consists of hornblende schist (Kc1), garnet hornblende gneiss (Kc2), garnet metadiorite (Kc3). Filled circles in Kc2 mark sites where UHP ultramafic rocks were observed or sampled from boulders. Open circles in Kc2 and Kc3, mark sites where eclogite was sampled. Samples DR05-2 and DR00-6, referred to in the paper, are respectively from the westernmost and easternmost locations. The Cuaba terrane is intruded by the Río Boba intrusive suite (g). Younger sedimentary rocks and sediment are Upper Eocene-Miocene clastic sedimentary rocks (Tcs), Neogene limestones (Tl), and Quaternary alluvium (Q). Reverse faults: bold, toothed lines (teeth, on hang wall). Left-laterals strike slip faults: bold un-ornamented lines, dashed where uncertain. "San Francisco de Macoris" is the closest, major city. "Cuevas" is the village closest to the principal occurrences of Grt ultramafic rock.

consists of serpentinite and blueschist-eclogite melange with serpentine matrix, faulted against fine-grained, coherent greenschist-blueschist facies rocks. The HP/low temperature (LT) metamorphism of these rocks is interpreted as having resulted from SW-directed subduction in the Cretaceous (Draper and Nagle, 1991; Draper *et al.*, 1994; Krebs *et al.*, 2008). The southern part of the Río San Juan metamorphic complex consists of the Cuaba terrane and the Río Boba intrusive suite (Fig. 1). The Cuaba terrane is predominantly hornblende gneiss and hornblende schist. The common mineral assemblage is Hbl + Pl(andesine) + Qtz + Rt + /-Grt + /-Bt + /-Ep. Draper and Nagle (1991) suggested a mafic protolith (basalt/diabase/gabbro) of ocean-crustal origin. Preliminary whole rock chemical analyses (Appendix) indicate a MORB provenance for unit Kc2 (Fig. 1). A more comprehensive trace-element data-set (Escuder-Viruete, 2009) points to a MORB provenance for some samples from this same unit (Kc2, Fig. 1). The unpublished data also identify a strong island-arc tholeiite (IAT) component in all three units of the Cuaba terrane.

Retrograded eclogite in the unit Kc2 (Fig. 1) of the Cuaba terrane was first reported in 1998 (Abbott and Draper, 1998). Evidence for eclogite is in the form of Pl-Di symplectite + Grt, with greater or lesser amounts of hornblende depending on the extent of retrograde hydration (Abbott and Draper, 1998, 2002). The retrograded eclogite occurs as mm- to dm-scale layers in otherwise symplectite-free hornblende gneiss. Retrograde eclogite has also been identified in unit Kc3, but not in unit Kc1. Garnet peridotite was first reported in 2001 (Abbott *et al.*, 2001). The garnet-bearing ultramafic rock, and related olivine clinopyroxenite and clinopyroxene garnetite occur as stream boulders that have weathered out of the Cuaba terrane. The Cuaba terrane was intruded by gabbroic to quartz dioritic rocks of the Río Boba intrusive suite (Draper and Nagle, 1991). The petrogenetic relationship (if any) between the HP/LT rocks in the northern part of the inlier and HP/UHP rocks of the Cuaba terrane remains unclear.

ULTRAMAFIC ROCK

Garnet ultramafic rock and related olivine clinopyroxenite are of plutonic, igneous origin (dikes, Fig. 2; cumulate texture, Fig. 3) and document a series of mineral assemblages related by fractional crystallization (Abbott *et al*., 2005, 2006b, 2007). Except for one deeply weathered, *in situ* exposure, all observations and samples of the ultramafic rock come from stream boulders (up to 5m) that have been weathered out of the adjacent gneiss. Field relationships inferred from the boulders (Fig. 4) and phase relationships (Fig. 5, Abbott *et al*., 2005, 2006b, 2007) indicate the following mineral assemblages, preserved as the products of fractional crystallization, from high temperature to low temperature:

I. Olivine clinopyroxenite (Fig. 2): Cpx + Ol + Opx + Mag + (retrograde Cr-Spl + Hbl + Srp),

II. Garnet olivine clinopyroxenite: Cpx + Ol + Grt + (retrograde Hbl + Srp),

III. Garnet peridotite: Cpx + Ol + Grt + Spl + (retrograde Hbl + Srp),

IV. Garnet clinopyroxenite and dikes of clinopyroxene garnetite (Fig. 2): Cpx + Grt + Spl + (retrograde Hbl),

V. Corundum-bearing garnet clinopyroxenite (Fig. 3): Cpx + Grt + Spl + Crn + (retrograde Hbl).

Magmatic conditions

The original estimates of magmatic conditions (P>3.4GPa and T>1550°C, Abbott *et al*., 2005, 2006b, 2007) were based on experimental determinations in two simple systems, relating respectively to the following:

1) The stability of sapphirine at high pressure. The sapphirine-out reaction Spr=Grt + Spl + Crn in the MAS system (Ackermand *et al*., 1975) defines the minimum pressure for the observed assemblage Grt + Spl + Crn.

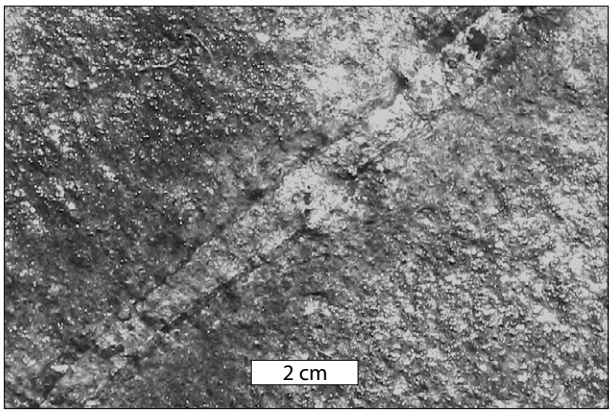

FIGURE 2 | Field photograph of a narrow dike of clinopyroxene garnetite (assemblage IV, Grt + Cpx + Spl + late Hbl) cutting olivine clinopyroxenite (assemblage I, Cpx + Ol + Opx + late Hbl + late Srp). Note the dark, ~2-mm selvage of Hbl at the margins of the dike.

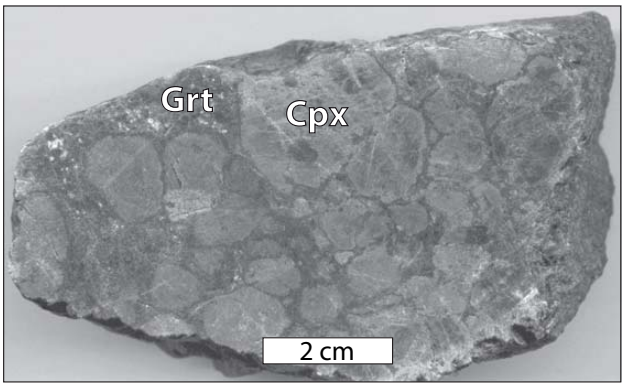

FIGURE 3 | Corundum-bearing garnet clinopyroxenite (DR03-12, assemblage V, Cpx + Grt + Spl + Crn + late Hbl). The dominant features of the rock are megacrysts of orthocumulate clinopyroxene (light gray euhedral to subhedral phenocrysts) and interstitial garnet. Spinel occurs as fine (<1mm), inclusions in garnet. The fine, white inclusions in garnet are corundum. Hornblende forms thin (1mm) selvages on phenocrysts of clinopyroxene. The hornblende is interpreted as the product of late, retrograde hydration.

2) The solidus for garnet peridotite and garnet clinopyroxenite. High pressure (3GPa) melting experiments in the CMAS system (Milholland and Presnall, 1998) show a stability field for sapphirine, which at higher pressure must disappear where the solidus intersects the sapphirine-out reaction.

The minimum P-T conditions for melt coexisting with Grt + Spl + Crn (+ Cpx) correspond to the intersection of the garnet clinopyroxenite (+ Spl + Crn) solidus and the sapphirine-out reaction, Spr=Grt + Spl + Crn (Abbott *et al*., 2005, 2006b, 2007; Gazel *et al*., 2011). In the CMAS system, the conditions at this intersection are P~3.4GPa, T~1550°C (open circle in Fig. 6).

The influence of non-CMAS components (esp., Fe and Na) was explored in Gazel *et al*. (2011), who offered revised solidus conditions of P>3.2GPa and T>1500°C (filled circle in Fig. 6), a little lower in P and T than the original estimates. The revised conditions take into account non-MAS components in the sapphirine-out reaction, and use the experimentally determined solidus for natural compositions of garnet peridotite/clinopyroxenite (Walter, 1998; Herzberg *et al*., 2000; Hirschman, 2000).

Fe-Mg partitioning between spinel and garnet coexisting with olivine (Abbott *et al*., 2007; Gazel *et al*., 2012) is consistent with temperatures up to ~1340°C. Rare earth element (REE) values for the garnet are consistent with temperatures up to 1475°C (Gazel *et al*., 2011, 2012, and see below), approaching magmatic conditions at P>3GPa

Subsolidus P-T conditions: Garnet peridotite–garnet clinopyroxenite

Representative mineral chemistries are reported in Table 1 for garnet peridotite, sample DR03-10

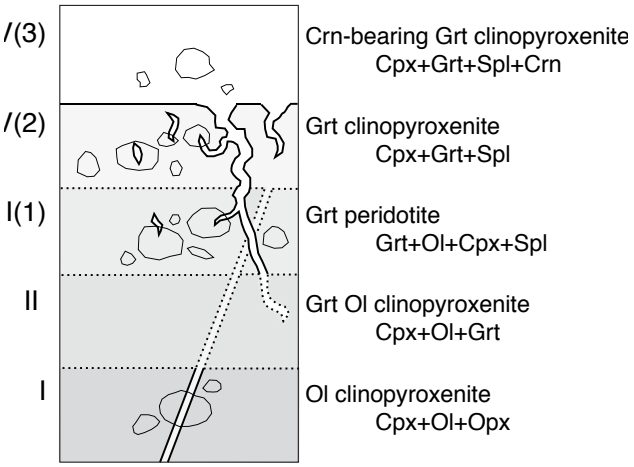

FIGURE 4 | Schematic intrusive relationships (Abbott *et al.*, 2007). Observed contacts are solid; inferred contacts are dotted. Irregular, closed loops are meant to represent the different kinds of boulders. The relative dimensions of the various features are not drawn to any particular scale. Boulders range in size up to 5m. Veins and segregations of Crn-bearing Grt clinopyroxenite, assemblage V(3), are typically on a decimeter scale. Straight dikes of Grt clinopyroxenite, assemblage IV(2), range in width up to 4 cm (see 1-2 cm example in Fig. 2).

(reproduced from Abbott *et al*. 2006a). Chemical analyses of hornblende were performed by electron microprobe, wavelength dispersion spectroscopy (WDS) (Florida International University, Table 1). Chemical analyses of garnet, and olivine were performed by scanning electron microscope (SEM), energy dispersion spectroscopy (EDS) (Appalachian State University, Table 1), and by electron microprobe, WDS (Florida International University, Table 1). Comparing the analyses by the two methods indicates that the SEM-EDS analyses are of adequate quality for the purpose of thermodynamic calculations involving major elements. In those minerals for which vacancies are negligible (*i.e.*, Grt, Spl, Ol, Cpx), chemical formulae were normalized on the basis of cations per formula unit (p.f.u.). Otherwise, the SEM-EDS analyses provide reasonable stoichiometries, *e.g.*, (Ca + Mg + Mn + Fe)~3 in Grt, Al~2 in Spl, and Si~1 in Ol. The chemical formula for hornblende was calculated by the computer program AX (Holland and Powell, 2000), which provides an estimate of Fe^{3+} .

Temperatures were calculated (Abbott *et al*., 2006a) for Fe-Mg exchange between garnet and clinopyroxene. Figure 7 shows the results for Ai's (1994) Fe-Mg exchange model, which agrees most closely with THERMOCALC. At 3.5GPa, the calculated temperature is ~900°C (Abbott *et al*., 2006a). The estimated temperature relates to subsolidus closure for Fe-Mg exchange between garnet and clinopyroxene.

Average P-T conditions were calculated for garnet peridotite (III, Ol + Grt + Cpx + Spl) using THERMOCALC, v. tc325, data set 5.5, 12 November 2004 (Holland and Powell, 1998; Powell *et al*., 1998; Powell, 2005). Activities of mineral components in garnet (grs, prp, alm) coexisting with spinel, olivine (fo, fa), and clinopyroxene (di, hd) were calculated using the program AX (Holland and Powell, 2000). The activities of spl and hc were calculated for disordered spinel (Pavese *et al*., 1999), using a standard first approximation formulation (*e.g.*, see Spear, 1993), $a_{spl}^{Spl} \sim X_{Mg}^{Spl}(1/3)_{Tet.}(2/3)^2_{Oct.}$, where $X_{Mg}^{Spl}=Mg/(Mg + Fe^{2+})$; and $a_{hc}^{Spl} \sim X_{Fe}^{Spl}(1/3)_{Tet.}(2/3)^2_{Oct.}$, where $X_{Fe}^{Spl}=Fe^{2+}/(Mg + Fe^{2+})$. The large, filled circle in Figure 7 marks the calculated conditions of P=3.4(+/-0.7)GPa and T=838(+/-170)°C, where the uncertainty expresses the standard deviation (error bars in Fig. 7). The conditions are consistent with approximately isobaric cooling from magmatic conditions.

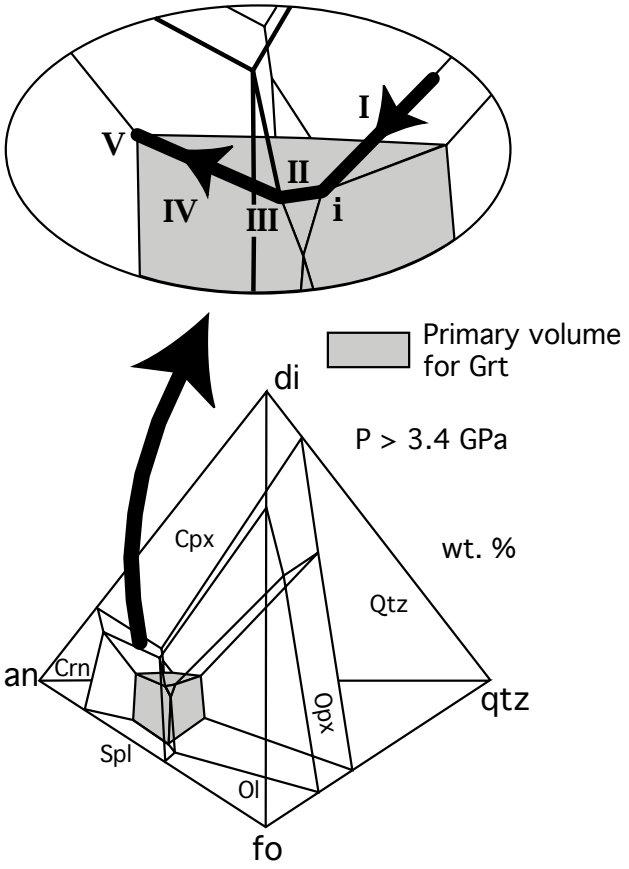

FIGURE 5 | Primary liquidus volumes for mineral-phases in a portion of the CMAS system at P>3.4GPa (Abbott *et al.*, 2005, 2006b, 2007, as modified from Milholland and Presnall, 1998). Primary liquidus volume for garnet is highlighted. Details emphasizing liquids saturated with Cpx are shown in the inset. Liquids on the bold line correspond to minerals assemblages I, II, III, IV and V, as indicated. Point "i" marks the Liq in the equilibrium, Ol + Cpx + Grt=Opx + Liq. Segment II is the locus of Liq in the equilibrium, Ol + Cpx + Grt=Liq. Point III marks the Liq in the equilibrium Cpx + Spl=Grt + Ol + Liq. Segment IV is the locus of Liq in equilibrium with Cpx, Grt and Spl. Point V marks the Liq in the equilibrium Cpx + Grt + Crn = Spl + Liq.

TABLE 1 | Garnet peridotite, DR03-10, Mineral Analyses

Mineral	Grt[1]	Grt[1]	Grt[2]	Spl	Ol	Ol	Cpx	Hbl[3]
Lab	ASU[4]	FIU[5]	ASU	ASU	ASU	FIU	FIU	FIU
No. of Analyses	5	4	5	14	5	5	22	5
				wt%				
SiO_2	39.4	38.86	39.08	0.48	38.28	37.62	50.90	46.95
TiO_2	0.12	0.01	0.16	0.13	0.15	0.00	0.19	0.48
Al_2O_3	22.34	22.57	22.49	63.03	0.68	0.03	2.47	11.40
FeO	18.63	21.10	17.23	19.41	21.23	23.21	5.29	7.09
MnO	0.27	0.81	0.26	0.10	0.16	0.23	0.15	0.05
MgO	10.24	9.47	8.06	16.55	39.15	40.12	15.49	16.48
CaO	9.01	8.57	12.72	0.30	0.35	0.01	23.05	12.48
K_2O	n/a[6]	0.00	n/a	n/a	n/a	0.00	0.00	0.00
Na_2O	n/a	0.00	n/a	n/a	n/a	0.00	0.12	1.49
Total	100.00	101.40	100.00	100.00	100.00	101.27	97.76	96.99
				Cations p.f.u.[7]				
Si	2.96	2.90	2.95	0.01	0.99	0.96	1.90	6.73
Al	1.98	1.99	2.00	1.92	0.02	0.00	0.12	1.93
Ti	0.01	0.00	0.01	0.00	0.00	0.00	0.01	0.05
Fe_T	1.17	1.32	1.09	0.42	0.46	0.49	0.16	0.85
Mn	0.02	0.05	0.02	0.00	0.00	0.00	0.00	0.01
Mg	1.15	1.05	0.91	0.64	1.51	1.53	0.87	3.52
Ca	0.73	0.69	1.03	0.01	0.01	0.00	0.93	1.92
K	n/a	0.00	n/a	n/a	n/a	0.00	0.00	0.00
Na	n/a	0.00	n/a	n/a	n/a	0.00	0.01	0.41
Total	8.00	8.00	8.00	3.00	3.00	2.98	4.00	15.41
$Mg\#_R = 100*Mg/(Mg+Fe_T)$	49	44	45	60	77	76	84	81
Fe^{3+}	0.09	0.21	0.08	0.05	0.00	0.12	0.03	0.12
Fe^{2+}	1.08	1.11	1.01	0.36	0.46	0.37	0.13	0.57
$Mg\#_O = 100*Mg/(Mg+Fe^{2+})$	51	49	47	64	77	81	87	86
prp[8]	0.37	0.34	0.30					
grs	0.24	0.22	0.34					
sps	0.01	0.02	0.01					
alm	0.38	0.42	0.36					
spl				0.64				
hc				0.34				
mag				0.03				
di+hd							0.85	
Ca-ts[9]							0.08	
jd+acm							0.01	
en+fs							0.07	

[1]Garnet next to inclusions of spinel.
[2]Garnet associated with hornblende, well away from spinel.
[3]Cations per formula unit for Hbl calculated by computer program AX, which estimates Fe^{3+}.
[4]ASU, analyses were performed by SEM-EDS at the College of Arts and Sciences Microscope Facility, Appalachian State University Garnet standard #5 (NBS 110752).
[5]FIU, analyses were performed at Florida Center for Analytical Electron Microscopy, Florida International University.
[6]n/a = not analyzed.
[7]p.f.u. = per formula unit.
[8]The quantity entered for each component species is the mole fraction.
In the case of garnet the species were calculated as follows:
prp = $Mg/(Mg+Ca+Mn+Fe_T)$, grs = $Ca/(Mg+Ca+Mn+Fe_T)$, sps = $Mn/(Mg+Ca+Mn+Fe_T)$, alm = $Fe_T/(Mg+Ca+Mn+Fe_T)$.
[9]Ca-ts = $CaAl_2SiO_6$.

Temperatures were also calculated for Fe-Mg exchange between garnet and hornblende, using the model of Graham and Powell (1984). The results are shown in Figure 7 as the vertical bar terminating at 2.5GPa, the approximate upper pressure limit for hornblende (Abbott *et al*., 2007).

The proposed P-T path is shown in Figure 7 (dotted). The ultramafic rock was dragged to the subduction zone by forced convection in the mantle wedge (corner-flow), coupled with erosion of the hanging wall. Models of such flow (*e.g.*, Gerya *et al*., 2002; Gorczyk *et al*., 2007; Roselle

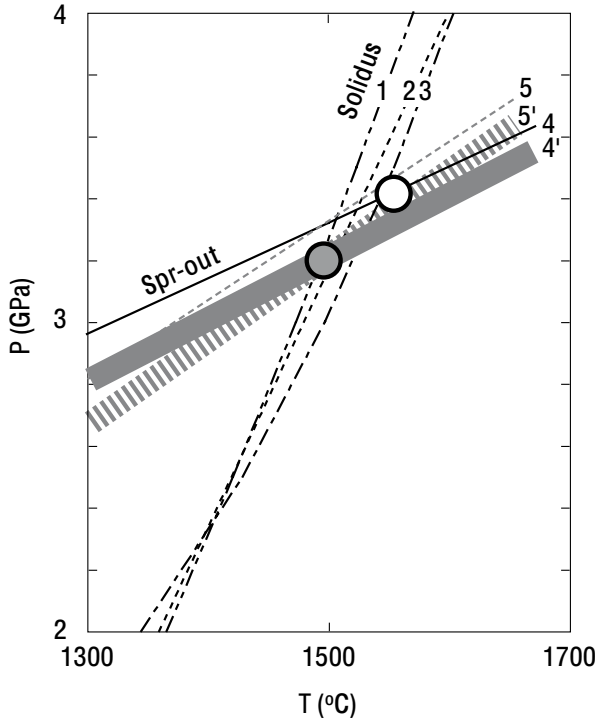

FIGURE 6 | Minimum P-T conditions for garnet peridotite magma (Gazel *et al.*, 2011). Previously estimated, minimum P-T conditions (open circle, ~3.4GPa, ~1550°C, Abbott *et al.*, 2005, 2006b) refer to the CMAS system. The new estimate of the minimum P-T conditions (filled circle, ~3.2GPa, ~1500°C, Gazel *et al.*, 2011) takes into account the effects of non-CMAS components and tschermak substitution. Experimentally determined garnet peridotite solidus: 1=Hirschmann (2000), 2=Walter (1998), 3=Herzberg *et al.* (2000). Experimentally determined sapphirine-out reaction: 4 (solid line)=MAS system (Ackermand *et al.*, 1975), and 4' (wide, solid band)=adjusted for Mg# of hypothetical sapphirine coexisting with the observed composition of spinel. THERMOCALC results for sapphirine-out reaction: 5 (dashed)=sapphirine of composition $Mg_{3.5}Al_9Si_{1.5}O_{20}$, and 5' (wide, dashed band)=adjusted for hypothetical Mg# of sapphirine coexisting with the observed composition of spinel.

et al., 2002) suggest cooling at constant or increasing pressure. The envisioned path involves approximately isobaric (P>3.2GPa, *e.g.*, 3.5GPa in Fig. 7) cooling from solidus conditions (~1500°C) down to ~900°C (Abbott *et al.*, 2006a; Abbott and Draper, 2007, 2008; Gazel *et al.*, 2011). At the subduction zone, the ultramafic rock was incorporated into, or otherwise mixed with, deep-subducted oceanic crust (eclogite).

Three generations of garnet

Abbott and Draper (2008) and Gazel *et al.* (2011) characterized three generations of garnet in the garnet clinopyroxenite, assemblage V (Cpx + Grt + Spl + Crn, sample DR03-12). The three generations are compositionally and texturally distinct: Grt[1], 29<grs<33, Fe>Ca, adjacent to Spl + Crn; Grt[1'], 37<grs<47, Fe~Ca, away from Spl, Crn, Cpx and Hbl; and Grt[2], 33<grs<42, Fe~Ca, associated with Hbl and Cpx. Phase relationships modeled on 3-GPa experimental data (Abbott *et al.*, 2005, 2006b, 2007; Abbott and Draper, 2008; Gazel *et al.*, 2011) show the following: The composition of Grt[1] is consistent with solidus or near solidus conditions, >3.2GPa. The composition of Grt[1'] is consistent with having formed isochemically from solidus or near solidus, high-Al clinopyroxene (Ca-ts~0.5, *i.e.*, approximately isochemical with Grt). Grt[2] formed late, under crustal conditions in conjunction with the formation of hornblende and final adjustments to the composition of clinopyroxene. The observed low-Al clinopyroxene is interpreted as the reequilibrated cores of originally magmatic clinopyroxene (early crystallized, Ca-ts<0.5, *i.e.*, less aluminous than Grt).

The three types of garnet are also distinct in terms of REEs (Gazel *et al.*, 2011). New data on the garnet (Gazel *et al.*, 2011) show "humped" or "sinusoidal" REE patterns, typical of garnet from acknowledged UHP settings (*i.e.*, garnet in kimberlite, and microinclusions of garnet in diamond). The peak of the "hump" in the normalized REE patterns for Grt[1] and Grt[1'] is at Eu (Dromedary-style).

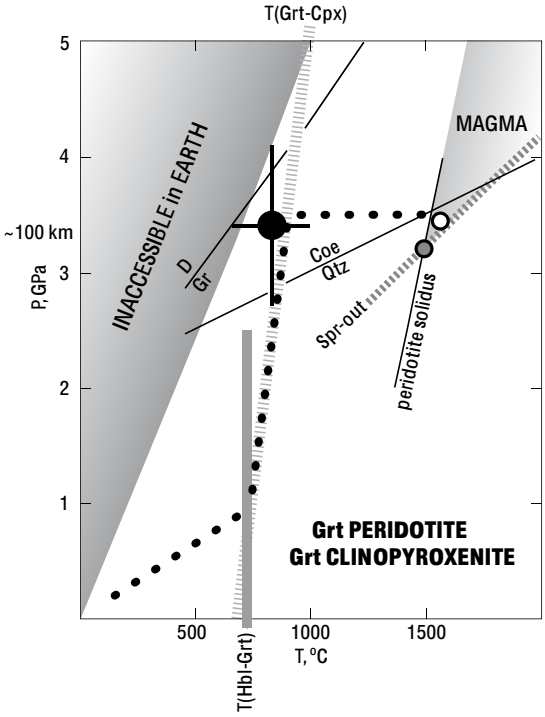

FIGURE 7 | P-T conditions for Grt-bearing ultramafic rock and proposed P-T path (bold, dotted). The shaded region (P >3.2GPa, T >1500°C, Gazel *et al.*, 2011) defines the magmatic conditions for the garnet ultramafic rock (Fig. 6). The small, gray-filled circle marks the new estimate of the minimum P-T conditions (Fig. 6). The small, open circle marks previously estimated, minimum P-T conditions (Abbott *et al.*, 2005, 2006b). The large, filled circle (with error bars, st. dev.) represents THERMOCALC results for the subsolidus equilibrium involving Grt + Spl + Cpx + Ol. Results of Cpx-Grt thermometry (Ai, 1994) are represented by the steep dashed band. Results of Grt-Hbl thermometry are represented by the vertical bands, terminating at ~2.5GPa, the approximate upper pressure limit for hornblende. D/Gr, diamond-graphite; Coe/Qtz, coesite-quartz.

The normalized REE patterns for Grt[2] show two peaks (Bactrian camel-style), at Sm and Gd on either side of Eu, such that the pattern has a small negative Eu anomaly on an otherwise upwardly convex pattern. The partitioning of REEs between Grt[1'] and Grt[1] is consistent with the former having inherited its REEs from a high-Al clinopyroxene predecessor of UHP magmatic origin (Gazel *et al*., 2011, 2012). As such, the partitioning of REEs between Grt[1'] and Grt[1] is consistent with temperatures approaching magmatic conditions (Gazel *et al*., 2011, 2012).

An alternative, low-pressure (LP) hypothesis

Hattori *et al*. (2009, 2010a) offer the alternative view that the garnet-bearing ultramafic rocks were derived from a plagioclase-bearing protolith of island-arc origin at relatively shallow depths (crust). In this low-pressure (LP) hypothesis, the garnet was the product of metamorphism during subduction. The LP model (Hattori *et al*., 2009, 2010a) was originally predicated on i) a small positive Eu anomaly (Eu/Eu*=1.18-1.32) in the whole rock chemistry of two samples of garnet wehrlite (our garnet peridotite) and ii) the assumption that the trace element chemistry of the linopyroxene relates to magmatic conditions. Subsequent data on additional samples (Hattori *et al*., 2010b) show that the least altered sample (lowest LOI) actually shows a small negative Eu anomaly (Eu/Eu*=0.89). Our work (Abbott and Draper, 2008, 2010; Gazel *et al*., 2011) shows that the clinopyroxene is chemically equilibrated to late, retrograde crustal conditions (amphibolite facies). That is, the composition of the relict clinopyroxene (major elements and trace elements) no longer reflects magmatic conditions. The LP model disregards the evidence for UHP magmatic origin (Abbott and Draper, 2010; Gazel *et al*., 2011) by ignoring phase relationships (albeit complex), orthocumulate clinopyroxene textures, structural evidence (dikes, cross-cutting mineral segregations), systematic variation in mineral assemblage (liquid line of descent), and systematic variations in mineral compositions. Hypothetical, monotonically increasing (light to heavy) REE ratios for garnet, used by Hattori *et al*. (2010a) in their modeling, and critical to their argument, bear no resemblance to the actual garnet (Gazel *et al*., 2011). Gazel *et al*. (2011) indicate that any small, positive or negative, whole rock Eu anomaly can be accommodated by different amounts of the three types of garnet, Grt[1], Grt[1'] and Grt[2]. De Hoog (2012) commented on the UHP hypothesis, but none of his criticism precludes a UHP magmatic origin for the garnet ultramafic rocks (Gazel *et al*., 2012).

ECLOGITE

The typical eclogite (Fig. 8, DR05-2) is granoblastic to subtly foliated, depending on the amount of hornblende. In hand specimen, the granoblastic texture consists of subhedral to euhedral prophyroblasts of deep-red garnet set in an aphanitic gray-green matrix. Garnet porphyroblasts are typically <3mm, but can reach 7mm. Hornblende occurs in narrow (~0.5mm) selvages on the garnet and fills fractures in the larger garnets. Locally the hornblende is absent or scarce. The garnet prophyroblasts and matrix are in sub-equal proportions and collectively make up 85% or more of the rock.

Thin sections reveal important microscopic details. The narrow (~0.5mm) hornblende selvages on garnet resolve into a fine-grained intergrowth of hornblende, quartz and epidote. The aphanitic matrix resolves into a fine-grained (0.01-0.05mm) vermicular Pl-Cpx symplectite, referred to as type-I symplectite (Sym-I) in Abbott and Draper (2007). Minor minerals include Fe-Ti oxide, rutile, titanite, apatite, and pyrite. Titanite forms rims on the Fe-Ti oxide minerals (lower right corner, Fig. 8B). Small (~1mm),

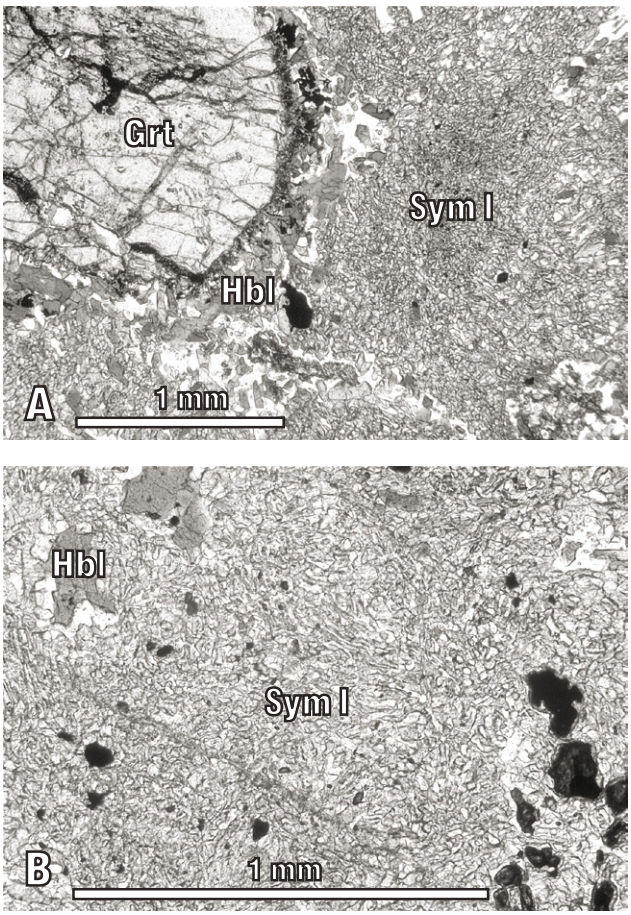

FIGURE 8 | Digital images of typical retrograded eclogite (sample DR05-2, plane polarized light). A) Porphyroblast of garnet rimmed by hornblende + quartz + plagioclase. The matrix consists of Pl-Cpx symplectite (Sym-I). B) Region of symplectite, showing the vermicular intergrowth of plagioclase and clinopyroxene. Note discrete grains of hornblende associated with quartz. The opaque mineral is Fe-Ti oxide, rimmed by titanite.

isolated aggregates of fine-grained epidote (~10modal%) are distributed throughout the matrix of type-I symplectite. The garnet contains micro inclusions of quartz, rutile, and epidote. Hornblende is interpreted to be the last product of retrograde hydration. Prior to the formation of hornblende, the rock consisted of Grt + Sym + Qtz + Ep + Rt + Fe-Ti oxide. The inferred highest-grade assemblage was Grt + Omp + Ky + Coe + Rt + Fe-Ti oxide (Abbott and Draper, 2007).

The most interesting manifestation of eclogite (Fig. 9, DR00-6) differs from the typical eclogite in possessing a second form of symplectite involving plagioclase and epidote, referred to as type-II symplectite (Sym-II) in Abbott and Draper (2007). Details become apparent in thin section and in SEM images. Where hornblende is scarce (Fig. 9A), the gray-green matrix resolves into two types of symplectite. Symplectite-I (Sym-I) consists of a fine-grained (~0.05mm) intergrowth of plagioclase and clinopyroxene. SEM images (Fig. 9B) reveal the second symplectite (Sym-II) to be an unusual intergrowth of microlaths (<0.005mm) of epidote in plagioclase. In Figure 9A, microsymplectite-II forms the narrow (~0.1mm), optically amorphous mantles on garnet porphyroblasts and on aggregates of epidote. The contact between symplectite-I and microsymplectite-II is sharp (Fig. 9B). Symplectite-I (Pl-Cpx) touches neither garnet nor aggregates of epidote, by virtue of intervening microsymplectite-II (Pl-Ep). Minor minerals include quartz, Fe-Ti oxides, titanite, rutile, and zircon. Most of the quartz is associated with hornblende or occurs as inclusions in the garnet. Irregular crystals of Fe-Ti oxide occur in symplectite-I (Fig. 9A) and are rimmed by titanite. Minute (<0.010mm) crystals of rutile and zircon form scarce inclusions in garnet. Hornblende is interpreted as the last product of retrograde hydration, after the formation of symplectite-I and symplectite-II. Prior to the formation of hornblende, the rock consisted of Grt + Sym-I + Sym-II + Ep + Qtz + Rt + Fe-Ti oxide.

Representative mineral chemistries are reported in Table 2 for eclogite sample DR00-6 (reproduced from Abbott and Draper, 2007). The analyses were performed by SEM-EDS. In those minerals for which vacancies are negligible (*i.e.*, Grt, Ep, Cpx, Pl), chemical formulae were normalized on the basis of total cations per formula unit (p.f.u.), including artifacts of using an omphacite standard (bracketed values in Table 2). The chemical formula for hornblende was calculated by the computer program AX (Holland and Powell, 2000). Fe^{3+} was estimated stoichiometrically for Cpx (6 O p.f.u.). All Fe in Ep was expressed as Fe^{3+} . All Fe in garnet was expressed as Fe^{2+}. Despite the poor quality of some of the analyses (bracketed values in Table 2), the analyses are adequate for the intended purposes of estimating the reintegrated composition of omphacite, and for compositional parameters used in thermodynamic calculations. This is justified by the internal consistency in the results of the thermodynamic calculations.

The two types of symplectite are believed to have formed from the decomposition of two types of omphacite, Omp-I from Sym-I (Pl-Cpx), and Omp-II from Sym-II (Pl-Ep). The compositions of the original omphacites were reintegrated (Abbott and Draper, 2007) from the components of the respective symplectites, acknowledging a wide range in the modal amount of plagioclase from 40% to 60% in each type of symplectite,

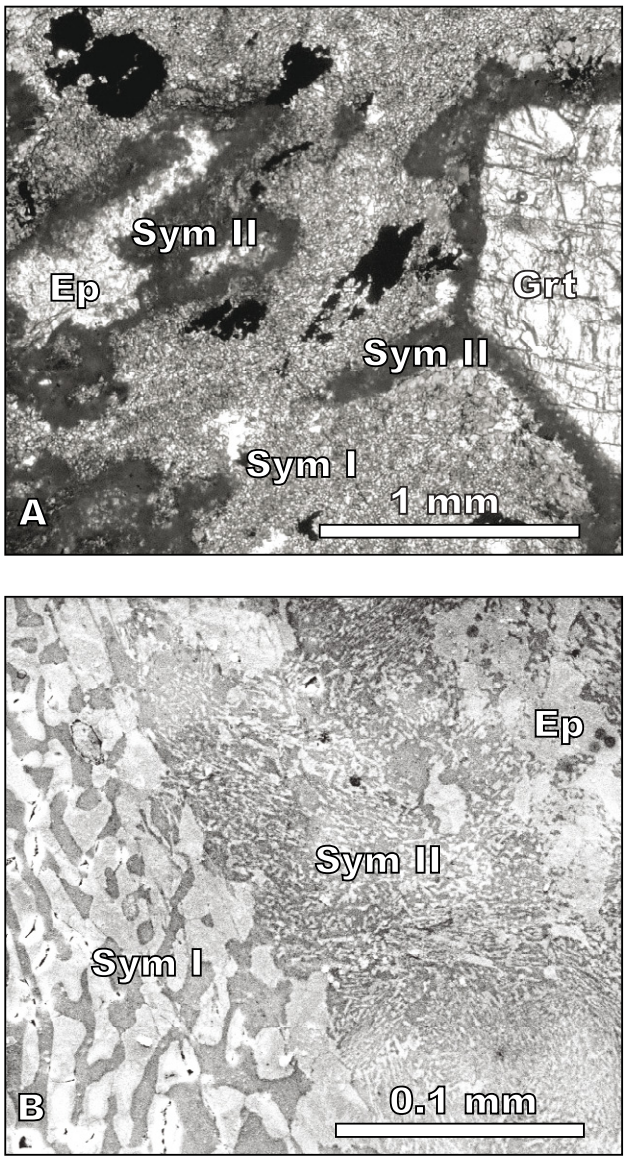

FIGURE 9 | Retrograded eclogite (sample DR00-6) with Pl-Cpx symplectite (Sym-I) and Pl-Ep symplectite (Sym-II). A) Digital image, plane-polarized light. The garnet porphyroblast and aggregate of epidote are each rimmed by optically amorphous symplectite-II (Pl-Ep). The matrix consists of Pl-Cpx symplectite (Sym-I). The opaque mineral is Fe-Ti oxide. B) SEM image showing Sym-I (Pl-Cpx) and Sym-II (Pl-Ep).

TABLE 2 | Eclogite, DR00-6[1,2], Mineral Analyses

	Symplectite, location 1		Symplectite, location 2				
Mineral:	Cpx	Pl	Cpx	Pl	Grt	Ep	Hbl[3]
No. of analyses	5	5	3	5	9	8	8
				wt%			
SiO_2	52.35	61.59	52.41	58.69	40.60	39.90	44.91
TiO_2	0.26	[0.14][4]	0.30	[0.14][4]	0.24	0.18	0.29
Al_2O_3	2.58	22.01	3.49	24.09	21.81	25.24	15.03
FeO	7.51	[0.82]	6.30	[1.09]	21.71	9.06	12.82
MnO	0.18	[0.11]	0.14	[0.15]	0.36	0.06	0.18
MgO	14.05	[0.93]	14.40	[1.48]	6.64	0.77	11.92
CaO	20.89	4.44	20.91	6.68	7.51	24.17	11.55
K_2O	0.13	0.13	0.06	0.06	[0.13]	0.13	0.13
Na_2O	2.04	9.83	1.99	7.63	[1.00]	0.50	3.17
Total	100.00	100.00	100.00	100.00	100.00	100.00	100.00
				Cations p.f.u[5]			
Si	1.91	2.71	1.91	2.61	3.09	3.02	6.40
Ti	0.01	0.00	0.01	0.00	0.01	0.01	0.03
Al	0.11	1.14	0.15	1.26	1.96	2.25	2.53
Fe_T	0.23	[0.03][4]	0.19	[0.04][4]	1.38	0.57	1.54
Mn	0.01	0.00	0.00	[0.01]	0.02	0.00	0.02
Mg	0.76	[0.06]	0.78	[0.10]	0.75	0.09	2.53
Ca	0.82	0.21	0.81	0.32	0.61	1.96	1.76
K	0.01	0.01	0.00	0.00	[0.01]	0.01	0.02
Na	0.14	0.84	0.14	0.66	[0.15]	0.07	0.88
TOTAL	4.00	5.00	4.00	5.00	8.00	8.00	15.71
$Mg\#_R = 100*Mg/(Mg+Fe_T)$	77		80		35		64
Fe^{3+}	0.20		0.16		0.00	0.57	0.12
Fe^{2+}	0.03		0.03		1.38		1.41
$Mg\#_O = 100*Mg/(Mg+Fe^{2+})$	96		97		35		62
di+hd[6]	0.73		0.72				
Ca-ts[7]	0.07		0.08				
Al-buf[8]	0.01		0.02				
jd+acm	0.15		0.14				
Ca-esk[9]	0.00		0.00				
en+fs	0.03		0.04				
ab+or (Si-Al)/2		0.78		0.67			
ab Na/(Na+Ca+K)		0.79		0.67			
prp					0.27		
grs					0.22		
sps					0.01		
alm					0.50		
ep						0.57	
czo						0.25	

[1]Note: Assemblage includes Qtz and minor Rt, Usp, Mag, Ap, Ttn.

[2]EDS standards: garnet (NBS 110752) and omphacite (NBS 110607).

[3]Cations per formula unit for Hbl calculated by computer program Ax, which estimates Fe^{3+}.

[4]Value in square brackets signifies an artefact of using the omphacite standard.

[5]p.f.u. = per formula unit.

[6]The quantity entered for each component species is the mole fraction.
In the case of garnet the species were calculated as follows:
prp = $Mg/(Mg+Ca+Mn+Fe_T)$, grs = $Ca/(Mg+Ca+Mn+Fe_T)$, sps = $Mn/(Mg+Ca+Mn+Fe_T)$, alm = $Fe_T/(Mg+Ca+Mn+Fe_T)$.

[7]Ca-ts, $CaAl_2SiO_6$.

[8]Al-buf = $CaMg_{1/2}Ti_{1/2}AlSiO_6$ (Al-Buffonite).

[9]$Ca_{1/2}[\ ]_{1/2}AlSi_2O_6$ (Ca-eskolaite).

and acknowledging observed variation in the composition of the plagioclase. The reintegrated composition for Omp-I is $(di + hd)_{45-30}Ca\text{-}ts_{4-1}Al\text{-}buf_{<1}(jd + acm)_{29-38}Ca\text{-}esk_{20-30}(en+fs)_{\sim1}$ with $Mg\#_{Omp\text{-}I}$76-85; the reintegrated composition for Omp-II is $(di+hd)_{25-17}Ca\text{-}ts_{26-14}Al\text{-}buf_0(jd + acm)_{25}Ca\text{-}esk_{26-34}(en + fs)_{<1}$ with $Mg\#_{Omp\text{-}II}$~14 (Abbott and Draper, 2007). For omphacite, Omp-I is unusual for its high content of Ca-esk, and Omp-II is unusual for its high content in Ca-ts and Ca-esk. The differences in the compositions suggest that Omp-I and Omp-II are

related by an "immiscibility gap". While the situation is complicated by high values for Ca-ts and Ca-esk, the combined effects of which are not known, the difference in the (di + hd) values for Omp-I and Omp-II suggests that the gap may be related to well-known high-temperature immiscibility gap between (di-hd) and (en-fs) (Davidson and Lindsley, 1985). Perhaps, Ca-ts and Ca-esk suppress the temperature of the "solvus". Alternatively, the compositional gap may be related to compositional gaps on the di-jd join (Davidson and Burton, 1987; discussed in Spear, 1993).

P-T conditions: Eclogite

This section presents a summary of P-T estimates for eclogite sample DR00-6 (Abbott and Draper, 2007). Results are portrayed in Figure 10 and compared with the P-T path for the garnet peridotite (Fig. 7). For each of the equilibria represented in Figure 10, the range of conditions reflects the uncertainty, especially with regard to the inferred composition of the original omphacites, Omp-I and Omp-II (for details, see Abbott and Draper, 2007).

Grt-Cpx thermometry: Eclogite

Temperatures were calculated using Fe-Mg exchange between garnet and clinopyroxene. Figure 10 shows the range of temperature using Ai's (1994) Fe-Mg exchange model for garnet paired with clinopyroxene in Sym-I (Table 2; Abbott and Draper, 2007).

THERMOCALC, v. tc325, data set 5.5, 12 November 2004 (Holland and Powell, 1998; Powell *et al*., 1998; Powell, 2005), Fe-Mg exchange thermometry was applied to garnet paired with Cpx in Sym-I and to garnet paired with hypothetical Omp-I, at two pressures, 1.5 and 3.0GPa. The lowest temperatures correspond to Grt paired with Omp-I_{40} (reintegrated from Sym-I of 40%Pl + 60%Cpx); the highest temperatures correspond to Grt paired with Omp-I_{60} (reintegrated from Sym-I of 60%Pl + 40%Cpx). The lowest THERMOCALC temperatures (Grt-Omp-I_{40}) are ~60°C (1.5GPa) to ~70°C (3GPa) lower than the lowest temperatures (Grt-Cpx) from Ai's (1994) model (Fig. 10). The highest THERMOCALC temperatures (Grt-Omp-I_{60}) are ~80°C (1.5GPa) to ~100°C (3GPa) lower than the highest temperatures (Grt-Cpx) from Ai's (1975) model (Fig. 10). The THERMOCALC temperatures (Grt-Omp and Grt-Cpx) overlap temperatures from Ai's (1975) model (Grt-Cpx), but the THERMOCALC temperatures form a narrower range, displaced to lower temperature relative to results using Ai's (1994) model, at any pressure. For the broad scale of conditions depicted in Figure 10, the difference is not significant.

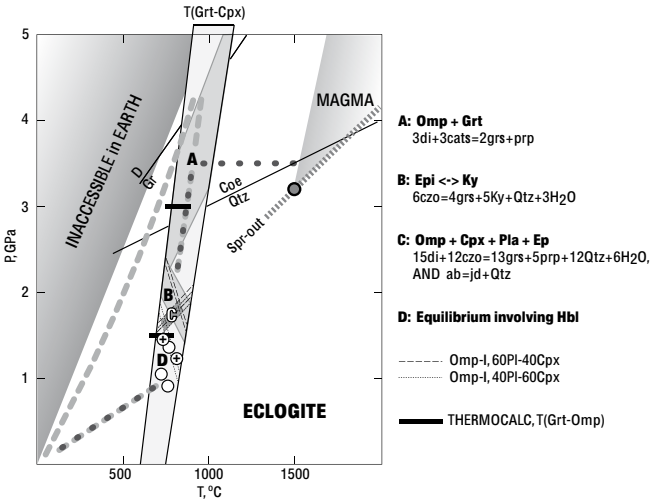

FIGURE 10 | P-T estimates based on garnet-clinopyroxene Fe-Mg exchange thermometry and other equilibria, described in the text. The proposed P-T path for the eclogite is shown by the bold, dashed, gray line. The proposed P-T path for the Grt-bearing ultramafic rock (Fig. 7) is shown as the bold, dotted line. D/Gr, diamond-graphite; Coe/Qtz, coesite-quartz.

Estimation of pressure, THERMOCALC: Eclogite

Pressures were estimated from the intersections of the Grt-Cpx thermometry and the following mineral equilibria:

1) $ab^{Pl}=jd^{Omp} + Qtz$
2) $15\ di^{Omp} + 12\ czo^{Ep}=13\ grs^{Grt} + 5\ prp^{Grt} + 12\ Qtz + H_2O$
3) $6\ czo^{Ep}=4\ grs^{Grt} + 5\ Ky + Qtz + 3\ H_2O$
4) $3\ di^{Omp} + 3\ Ca\text{-}ts^{Omp}=2\ grs^{Grt} + prp^{Grt}$

None of the equilibria involves Fe-components, thus they are largely independent of problems related to uncertainty in the oxidation state of Fe.

Equilibrium 1 was evaluated for hypothetical Omp-I paired with plagioclase. The calculations were referred to the extreme compositions of the type-I omphacite (Omp-I_{40}, reintegrated from 40%Pl + 60%Cpx, and Omp-I_{60}, reintegrated from 60%Pl + 40%Cpx) and extreme compositions for plagioclase (Table 2; Abbott and Draper, 2007). The restricted range of solutions is shown in Figure 10 as the positive-slope equilibria bounding the shaded region "C". Solutions to equilibrium 2 (negative-slope equilibria bounding shaded region "C") were evaluated for garnet, epidote (Table 2; Abbott and Draper, 2007) and the extreme compositions for Omp-I (Omp_{40}-Omp_{60}). The intersection of solutions to equilibrium 1 and equilibrium 2 (stable conditions for Grt + Omp-$I_{40\text{-}60}$ + Pl + Ep + Qtz + H_2O) defines the small P-T region labeled "C," P~1.5-1.9GPa and T~700-850°C. Agreement with the Grt-Cpx thermometry in Figure 10 is the principal reason for favoring Ai's (1994) formulation of the garnet-clinopyroxene thermometer.

Equilibrium 3 relates to the maximum pressure for the observed epidote (czo_{25}, Table 2) and also relates to the pressure above which kyanite is possible. Solutions for equilibrium 3 are represented by the shaded region labeled "B" in Figure 10. The equilibrium is independent of omphacite and plagioclase, and suggests slightly higher pressure than equilibria 1 and 2. Evidently, the decomposition of Omp-I to Sym-I took place under conditions consistent with the stability of epidote. Inasmuch as Sym-II consists of plagioclase and epidote, Omp-II and Omp-I must have decomposed under similar conditions.

Equilibrium 4 explores the stable coexistence of Omp-I + Omp-II + Grt (Abbott and Draper, 2007). THERMOCALC solutions for equilibrium 4 reside in the region labeled "A" in Figure 11. The low-pressure limit corresponds to the solution involving Omp-I_{47} (reintegrated from Sym-I_{47} of 47%Pl + 53%Cpx) and Omp-II_{40} (reintegrated from Sym-II_{40} of 40%Pl + 60%Ep). The high-pressure limit corresponds to the solution involving Omp-I_{57} (reintegrated from Sym-I_{57} of 57%Pl + 43%Cpx) and Omp-II_{60} (reintegrated from Sym-II_{60} of 60%Pl + 40%Ep). All possible solutions involving intermediate, equilibrium pairs of Omp-I and Omp-II, coexisting with garnet, reside between these extremes. Most of region "A" is between the quartz-coesite equilibrium and the graphite-diamond equilibrium (~2.8 to ~4.4GPa). The conditions compare favorably with subsolidus conditions for the garnet peridotite.

Finally, the "average P-T" option in THERMOCALC was used to estimate the equilibrium conditions for Hbl + Grt + Cpx + Pl + Qtz (open circles, Fig. 10), and for Hbl + Grt + Cpx + Ep + Pl + Qtz (circles with " + ", Fig. 10). None of the equilibria involved H_2O.

The proposed P-T history for the eclogite is indicated by the gray, dashed path in Figure 10. The prograde history remains speculative, but is presumed to have started with cooled basalt on the sea floor (Electronic Appendix available at www.geologica-acta.com). The proto-eclogite (sea floor basalt) was subducted to a depth as great as 120km (~4GPa). At the highest pressure, the assemblage would have been Grt + Omp-I + Ky + Coe + Rt + Fe-Ti oxide. The shaded region "A" relates to the retrograde assemblage, Grt + Omp-I + Omp-II + Ky + Coe + Rt + Fe-Ti oxide, and the formation of Omp-II according to a reaction of the form, Omp-II + Coe=Omp-I + Ky + /-Grt.

Details of the reaction are given in Abbott and Draper (2007). The region "B" relates to the retrograde appearance of epidote and consumption of kyanite. Region "C" corresponds to the breakdown of Omp-I to Sym-I (Pl + Cpx), and must also correspond closely to the breakdown of Omp-II to Sym-II (Pl + Ep). Circles "D" relate to the formation of retrograde hornblende. The inferred P-T path involved i) deep subduction of basalt to ~120km (~4GPa) and prograde metamorphism, ii) nearly adiabatic uplift to ~30km (~1GPa) and retrograde metmorphism, followed by iii) a final stage of uplift with accelerated cooling, perhaps mediated by H_2O, through crustal conditions. The sequence of retrograde mineral assemblages along the retrograde part of the dashed path in Figure 10 is illustrated in Figure 11 (from Abbott and Draper, 2007).

The sequence of retrograde mineral assemblages (Figs. 10; 11) is broadly consistent with phase relationships calculated by Wei and Clarke (2011) for a "standard" MORB composition. The comparison is worthwhile because the major-element composition of one sample of retrograded eclogite (DR05-6, Appendix) is very close to the MORB composition used by Wei and Clarke (2011). For practical purposes, sample DR05-6 (Appendix) is petrographically equivalent to sample DR05-2, described above (Fig. 8). The highest-grade mineral assemblages inferred for the Cuaba eclogite (P>region "B," Figs. 10; 11) correctly fall in Wei and Clarke's (2011) kyanite-eclogite field, but at temperatures higher than the maximum temperature of 700°C considered by Wei and Clarke (2011). On the retrograde P-T path for the Cuaba eclogite (Figs. 10; 11), hornblende appears at a lower pressure than the decomposition of the omphacite (Omp-I) to Pl-Cpx symplectite (Sym-I). This means that the retrograde P-T path for the Cuaba eclogite passes directly from Wei and Clarke's (2011) kyanite-eclogite field to their amphibolite field, without passing through their hornblende-eclogite field. This implies temperatures greater than 700°C, outside the range of temperature considered by Wei and Clarke (2011). While the retrograde P-T path for the Cuaba eclogite is broadly consistent with

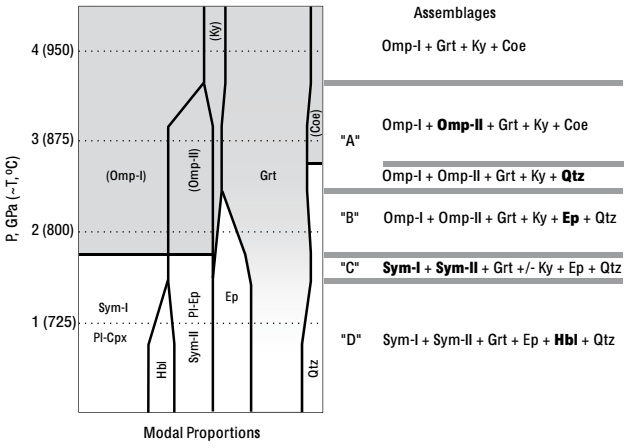

FIGURE 11 | Evolution of the mineral assemblage in DR00-6 along the retrograde path, designated by the bold, dashed gray line in Figure 10. Widths of the regions are qualitatively proportional to the modal amounts of the minerals.

Wei and Clarke's (2011) calculated phase diagrams, there are certain inconsistencies. For instance, in the region "B" in Figure 10 the maximum pressure for epidote is ~2.4GPa at ~700°C, whereas the maximum pressure for epidote in Wei and Clarke's (2011) kyanite-epidote field is ~2.5GPa at ~650°C. This discrepancy may reflect differences in fugacity of oxygen or activity of H_2O or both. Increased oxygen fugacity should expand the field for epidote to higher temperatures.

TECTONIC MODEL

The tectonic interpretation shown in Figure 12 (Abbott *et al*., 2006a) serves as a working hypothesis. The isobaric part of the P-T path for the garnet ultramafic rock took place in the mantle and involved delivery to the subduction zone in mid to Late Cretaceous time (1, Fig. 12). Garnet ultramafic rock of the mantle wedge was cooled and introduced into the deep-subducted oceanic crust (1', Fig. 12) in response to forced convection in the mantle wedge (corner flow) combined with erosion of the hanging wall of the subduction zone. The eclogite, with tectonic blocks of the garnet ultramafic rock onboard, was transported up the subduction channel (2, Fig. 12), perhaps by some variant of reverse flow as modeled for instance by Gerya *et al*. (2002) and Gerya and Yuen (2003). The mechanism is very poorly understood in the present context because of the great depths involved. Nevertheless, in an effort to explain the exhumation of the garnet peridotite in the Cuaba terrane, Gorczyk *et al*. (2007) developed a numerical model involving the upwelling of hydrated peridodite and partially molten peridotite, which in turn induces the upwelling of hot, presumably dry asthenosphere. In their numerical simulation UHP material (Cuaba terrane?) is introduced into, and transported up, the subduction channel from depths as great as ~120km (4GPa). However, Krebs *et al*. (2011) point out that the constraints used in Gorczyk's *et al*. (2007) simulation involve unrealistically slow rates of convergence (~25mm/a) and an unrealistically short duration of steady-state subduction (~18Ma). Whatever the mechanism, transport up the subduction channel was essentially completed prior to mid-crustal intrusion by dioritic to gabbroic rocks (Río Boba intrusive suite) of uncertain, but presumably Upper Cretaceous, age. The last part of the history relates to uplift through the crust to the surface (3, Fig. 12), completed by Mid-Eocene, perhaps in response to initiation of transcurrent tectonics (Mann *et al*., 1990; Pindell and Barrett, 1990; Draper *et al*., 1994, 1996; Pindell, 1994; Pindell *et al*., 2005).

CONCLUSIONS

Improved estimates of the magmatic conditions for the Dominican garnet peridotite–garnet clinopyroxenite

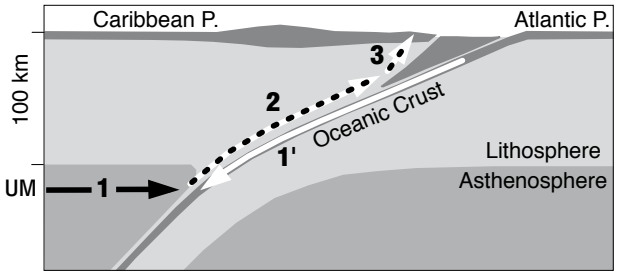

FIGURE 12 | Simplified plate tectonic interpretation. See text for discussion.

(>3.2GPa, >1500°C, Gazel *et al*., 2011) are slightly lower in P and T than previous estimates (~3.4GPa, ~1550°C, Abbott *et al*., 2005, 2006b). At P less than ~3.5GPa, the solidus is in the field of stability for quartz; at higher P, it is in the field of stability for coesite. The unique solidus assemblage of Grt + Spl + Crn(+ Cpx) does not necessarily indicate UHP conditions, because the solidus in the interval from ~3.2GPa to ~3.5GPa is in the stability field for quartz. However, even at the lowest pressure (~3.2GPa), subsolidus temperatures less than ~1250°C would be in the field of stability for coesite (Figs. 7; 10).

The great depth of origin of the garnet-bearing ultramafic rocks (>100km) and REE patterns for the garnet implicate an origin in the mantle. The very high temperatures for protoliths of the garnet-bearing ultramafic rocks (~1500°C) suggest that they are a product of mantle plume-head magmatism under UHP conditions (Gazel *et al*., 2011, 2012). Speculation favors the ancestral Galapagos plume (Kerr *et al*., 2003; Pindell and Kennan, 2009; Gazel *et al*., 2011).

Given the nature of forced convection (corner flow) in the mantle wedge (*e.g*., Gerya *et al*., 2002; Roselle *et al*., 2002), it is unlikely that the path of subsolidus cooling for the ultramafic rock could have escaped passing through the coesite field. Well away from the subduction zone, flow-lines in the mantle wedge are isobaric. Close to the subduction zone, flow-lines follow paths of increasing pressure in response to drag (draw-down) on the hanging wall of the subduction zone. Isobaric cooling all the way to the subduction zone would require unrealistically rapid erosion of the hanging wall. Even for this limiting situation, cooling from the minimum conditions (~3.2GPa, ~1500°C, Figs. 7; 10) for the original ultramafic magma passes through the coesite field. For isobaric cooling, the ultramafic rock would have been incorporated into the eclogite at P>3.2GPa and T>850°C, well within the coesite field. The equilibrium criterion $3di^{Cpx} + 3Ca\text{-}ts^{Cpx} = 2grs^{Grt} + prp^{Grt}$, applied to Grt + Omp-I + Omp-II in the eclogite (region "A", Fig. 10), is consistent with these conditions.

Subsolidus conditions related to near adiabatic decompression are the same for eclogite and the ultramafic rock. This supports the proposal that the ultramafic rock was delivered to the surface as tectonic blocks in the eclogite.

ACKNOWLEDGMENTS

The project is supported by National Science Foundation Grants EAR-8306145, EAR-8509542 and INT-0139536 to Draper and NSF Grants EAR-0111471 and INT-0139490 to Abbott. The research was supported by an Appalachian State University Research Grant to Abbott. We appreciate the time and assistance of the College of Arts and Sciences Microscope Facility, Appalachian State University, and director Dr. Guichuan Hou. The help and cooperation of the Dirección General de Minería and Ministerio del Medio Ambiente in the fieldwork associated with this project are greatly appreciated.

We appreciate the thoughtful reviews, comments and suggestions by Andrés Perez-Estaún, Walter Maresch, Javier Escuder-Viruete, and Pablo Ruiz.

REFERENCES

Abbott, R.N.Jr., Draper, G., 1998. Retrograde eclogite in the Cuaba Amphibolite of the Río San Juan Complex, northern Hispaniola [abs.]. Kingston (Jamaica) 15th Caribbean Geological Conference.

Abbott, R.N., Jr., Draper, G., 2002. Retrograded eclogite in the Cuaba Amphibolite of the Río San Juan Complex, Northern Hispaniola. In: Jackson, T.A. (ed.). Caribbean geology: into the third millennium: Transactions of the 15th Caribbean Geological Conference. The University of the West Indies Press, Kingston, Ch. 8, 97-108.

Abbott, R.N., Jr., Draper, G., 2007. Petrogenesis of UHP eclogite from the Cuaba Gneiss, Río San Juan complex, Dominican Republic. International Geology Review, 49, 1069-1093.

Abbott, R.N., Jr., Draper, G., 2008. Evolution of garnet and clinopyroxene in UHP ultramafic rock, Cuaba Gneiss, Río San Juan complex, Dominican Republic. Geological Society of America, Abstracts with Programs, 41(6), Abs. no.193-37, Houston.

Abbott, R.N., Jr., Draper, G., 2010. Comments on "Corundum-bearing peridotite from northern Dominican Republic: a metamorphic product of an arc cumulate in the Caribbean subduction zone", by Hattori *et al.* [Lithos 114 (2010) 437-450]. Lithos, 117, 322-326.

Abbott, R.N., Jr., Draper, G., Keshav, S., 2001. Garnet peridotite found in the Greater Antilles. EOS (Transactions of the American Geophysical Union), 82(35), 381-388.

Abbott, R.N., Jr., Draper, G., Keshav, S., 2005. UHP magma paragenesis, garnet peridotite and garnet clinopyroxenite: An example from the Dominican Republic. International Geology Review, 47, 233-247.

Abbott, R.N., Jr., Draper, G., Broman, B.N., 2006a. P-T path for ultra high pressure garnet ultramafic rocks of the Cuaba Gneiss, Río San Juan Complex, Dominican Republic. International Geology Review, 48, 778-790.

Abbott, R.N., Jr., Draper, G., Keshav, S., 2006b. UHP magma paragenesis, garnet peridotite and garnet clinopyroxenite: An example from the Dominican Republic. In: Liou, J. G., Cloos, M. (eds.). Phase relations, high-pressure terranes, P-T-ometry, and plate pushing: A tribute to W. G. Ernst. Bellwether Publishing, Ltd. for Geological Society of America, International Book Series, 9, 653-667.

Abbott, R.N., Jr., Broman, B.N, Draper, G., 2007. UHP magma paragenesis revisited, olivine clinopyroxenite and garnet-bearing ultramafic rocks from the Cuaba Gneiss, Río San Juan Complex, Dominican Republic. International Geology Review, 49, 572-586.

Ackermand, D., Seifert, F., Schreyer, W., 1975. Instability of sapphirine at high pressure. Contributions to Mineralogy and Petrology, 50, 79-92.

Ai, Y., 1994. A revision of the garnet-clinopyroxene Fe^{2+} -Mg exchange thermometer. Contributions to Mineralogy and Petrology, 115, 467-473.

Carswell, D.A., Compagnoni, R., 2003a. Introduction with review of the definition, distribution and geoteconic significance of ultrahigh pressure metamorphism. In: Carswell, D.A., Compagnoni, R. (eds.), Ultrahigh Pressure Metamorphism, European Mineralogical Union, 5, Eotvos University Press, Budapest, Ch. 1, 3-9.

Carswell, D.A., Compagnoni, R. (eds.), 2003b. Ultrahigh Pressure Metamorphism, European Mineralogical Union, 5, Eotvos University Press, Budapest, 508pp.

Davidson, P.M., Lindsley, D.H., 1985. Thermodynamic analyses of quadrilateral pyroxenes. Part II: Model calibration from experiments and application to geothermometry. Contributions to Mineralogy and Petrology, 91, 390-404.

Davidson, P.M., Burton, B., 1987. Order-disorder in omphacitic pyroxenes: A model for coupled substitution in the point approximation. American Mineralogist, 72, 337-344.

De Hoog, J.C.M., 2012, Comments on "Garnet-bearing ultramafic rocks from the Dominican Republic: Fossil mantle plume fragments in an ultra high pressure oceanic complex?" by Gazel *et al.* [Lithos 125 (2011) 393-404]. Lithos, 134-135, 330-334.

Draper, G., Nagle, F., 1991. Geology, structure, and tectonic development of the Río San Juan Complex, northern Dominican Republic. In: Mann P., Draper, G., Lewis, J.F. (eds.), Geologic and Tectonic development of the North American-Caribbean Plate Boundary in Hispaniola: Geological Society of America Special Paper, 262, 77-95.

Draper, G., Mann, P., Lewis, J.F., 1994. Hispaniola, In: Donovan, S.K., Jackson, T.A., (eds.), Caribbean Geology: An introduction. University of the West Indies Publishers' Association, Kingston, Jamaica, Ch. 7, 129-150.

Draper, G., Gutierrez, G., Lewis, J.F., 1996. Thrust emplacement of the Hispaniola peridotite belt: Orogenic expression of the mid-Cretaceous Caribbean arc polarity reversal? Geology, 24, 1143-1146.

Draper, G., Abbott, R.N., Jr., Keshav, S., 2002. Indication of UHP metamorphism in garnet peridotite, Cuaba Unit, Río San Juan Complex, Dominican Republic [abs.]. 16th Caribbean Geological Conference, Barbados.

Eberle, W., Hirdes, W., Muff, R., Pelaez, M., 1982. The geology of the Cordillera Septentrional (Dominican Republic). In: Snow, W., Gil, N., Llinas, R., Rodriguez-Torres, R., Tavares, I. (eds.), Transactions, 9th Caribbean Geological Conference: Santo Domingo, Dominican Republic, 1980, 619-632.

Escuder-Viruete, J., 2009. Petrología y Geoquímica de Rocas Igneas y Metamórficas (I y II): Hojas de Río San Juan, Guayabito, Salcedo, Gaspar Hernández, Pimentel, Cabrera y Villa Riva. Informe Complementario al Mapa Geológico de la República Dominicana a E. 1:50.000. Sysmin Project, IGME-BRGM, Santo Domingo, 163pp.

Escuder-Viruete, J., Friedman R., Castillo-Carrión, M., Jabites, J., Pérez-Estaún, A., 2011, Origin and significance of the ophiolitic high-pressure mélanges in the northern Caribbean convergent margin: Insights from the geochemistry and large-scale structure of the Río San Juan metamorphic complex. Lithos, 127, 483-504.

Gazel, E., Abbott, R.N., Jr., Draper, G., 2011. Garnet-bearing ultramafic rocks from the Dominican Republic: Fossil mantle plume fragments in an ultra high pressure oceanic complex? Lithos, 125, 393-404.

Gazel, E., Abbott, R.N., Jr., Draper, G., 2012, Reply to Comment on "Garnet-bearing ultramafic rocks from the Dominican Republic: Fossil mantle plume fragments in an ultra high pressure oceanic complex?" by Jan. C.M. De Hoog. Lithos, 134-135, 335-339.

Gerya, T.V., Stockert, B., Perchuk, A.L., 2002. Exhumation of high-pressure metamorphic rocks in a subduction channel: A numerical simulation. Tectonics, 21(6-6), 1056, doi: 10.1029/2002TC001406.

Gerya, T.V., Yuen, D.A., 2003. Rayleigh-Taylor instabilities from hydration and melting propel "cold plumes" at subduction zones. Earth and Planetary Science Letters, 212, 47-62.

Gorczyk, W., Guillot, S., Gerya, T.V., Hattori, K., 2007, Asthenospheric upwelling, oceanic slab retreat, and exhumation of UHP mantle rocks: Insights from Greater Antilles. Geophysical Research Letters, 34, L21309, doi:10.1029/2007/GL031059

Graham, C.M., Powell, R., 1984. A garnet-hornblende geothermometer: calibration, testing, and application to the Pelona Schist, southern California. Journal of Metamorphic Geology, 2, 13-21.

Hacker, B.R., McClelland, W.C., Liou, J.G. (eds.), 2006. Ultrahigh-pressure metamorphism: Deep continental subduction. Boulder, Colorado, Geological Society of America Special Paper, 403, 206pp.

Hastie, A.R., Ramsook, R., Mitchell, S.F. Kerr, A.C., Miller, I.L., Mark, D.F., 2010. Geochemistry of compositional distinct Late Cretaceous back-arc basin lavas: Implications for the tectonomagmatic evolution of the Caribbean plate. Journal of Geology, 118, 655-676.

Hattori, K., Tubrett, M., Saumur, B.-M., Guillot, S., 2009. Subduction of shallowly formed arc cumulates: Evidence from clinopyroxene compositions of garnet peridotites in the Río San Juan complex, northern Dominican Republic. Geophysical Research Abstracts, 11, EGU2009-6237.

Hattori, K.H., Guillot, S., Saumur, B.-M., Tubrett, M.N., Vidal, O., Morfin, S., 2010a. Corundum-bearing garnet peridotite from northern Dominican Republic: A product of an arc cumulate in the Caribbean subduction zone. Lithos, 114, 437-450.

Hattori, K.H., Guillot, S., Tubrett, M.N., Saumur, B.-M., Vidal, O., Morfin, S., 2010b. Reply to Comments on "Corundum-bearing garnet peridotites from northern Dominican Republic: A metamorphic product of an arc cumulate in the Caribbean subduction zone" by Richard N. Abbott and Grenville Draper. Lithos, 117, 327-330, doi:10.1016/j.lithos.2010.03.007.

Herzberg, C., Raterron, P., Zhang, J., 2000. New experimental observations on the anhydrous solidus for peridotite KLB-1. Geochemistry, Geophysics, Geosystems, 1(10), 1051, doi: 10.1029/2000GC000089.

Hirschmann, M.M., 2000. Mantle solidus: Experimental constraints and effects of peridotite composition. Geochemistry, Geophysics, Geosystems, 1(10), 1042, doi: 10.1029/2000GC000070.

Holland, T.J.B., Powell R., 1998. An internally consistent thermodynamic data set for phases of petrologic interest. Journal of Metamorphic Geology, 16, 309-343.

Holland, T.J.B., Powell, R., 2000. AX, Mineral activity calculation for thermobarometry. Cambridge University, Cambridge, computer program AX2 v. 2.2.

Jansma, P.E., Mattioli, G.S., Lopez, A., DeMets, C., Dixon, T.H., Mann, P., Calais, E., 2000. Neotectonics of Puerto Rico and the Virgin Islands, northeastern Caribbean, from GPS geodesy. Tectonics, 19, 1021-1037.

Kerr, A.C., White, R.V., Thompson, P.M.E., Tarney, J., Saunders, A.D., 2003. No oceanic plateau–no Caribbean plate? The seminal role of an oceanic plateau in Caribbean plate evolution. In: Bartolini, C., Buffler, R.T., Blickwede, J., eds., The Circum Gulf of Mexico and Caribbean: Hydrocarbon Habitats, Basin Formation, and Plate Tectonics, American Association of Petroleum Geologists Memoir, 79, 126-268.

Krebs, M., Maresch, W.V., Schertl, H.-P., Munker, C., Baumann,, A., Draper, G. Idleman, B., Trapp, E., 2008. The dynamics of intra-oceanic subduction zones: A direct comparison between fossil petrological evidence (Río San Juan Complex, Dominican Republic) and numerical simulation. Lithos, 103, 106-137.

Krebs, M., Schertl, H.P., Maresch, W.V., Draper, G., 2011, Mass flow in serpentine-hosted subduction channels: P-T-t path

patterns of metamorphic blocks in the Río San Juan mélange (Dominican Republic). Journal of Asian Earth Sciences, 42, 569-595.

Kretz, R., 1983. Symbols for rock-forming minerals. American Mineralogist, 68, 277-279.

Lewis, J.F., Draper, G., 1990. Geology and tectonic evolution of the northern Caribbean region, In: Dengo, G., Case, J.E. (eds.), The Caribbean Region: Boulder, Colorado, Geological Society of America, Geology of North America, H, 77-140.

Lieberman, J.E., Till, A.B., 1987. Possible crustal origin of garnet lherzolite: Evidence from the Kigluaik Mountains, Alaska. Geological Society of America Abstracts with Programs, 19(7), 746.

Liou, J.G., Cloos M. (eds.), 2006. Phase relations, high-pressure terranes, P-T-ometry, and plate pushing. Boulder, Colorado, Geological Society of America, International Book Series, 9, 667pp.

Liou, J.G., Tsujimori, Zhang, R.Y., Katayama, I., Maruyama, S., 2006. Global UHP metamorphism and contineentaal subduction/collision: The Himalayan model, In: Liou, J.G., Cloos M. (eds.), Phase relations, high-pressure terranes, P-T-ometry, and plate pushing. Boulder, Colorado, Geological Society of America, International Book Series, 9, 23-79.

Mann, P., Schubert C., Burke, K., 1990. Review of Caribbean neotectonics, In: Dengo, G., Case, J.E. (eds.), The Caribbean Region: Boulder, Colorado, Geological Society of America, Geology of North America, H, 307-338.

Mann, P., Calais, E., Ruegg, J.-C., DeMets, C., Jansma, P.E., Mattioli, G.S., 2002. Oblique collision in the northeastern Caribbean from GPS measurements and geological observations. Tectonics, 21(6-7), 1057, doi:10.1029/2001TC001304.

Mann, P., Rogers, R., Gahagan, L.M., 2007. Overview of plate tectonic history and its unresolved tectonic problems, In: Bundschuh, J., Alvarado, G., eds., Central America: geology, resources, and natural hazards. London, Taylor & Francis, 201-237.

MacKenzie, J.M., Canil, D., Johnston, J.E., English, J., Mihalynuk, M.G., Grant, B., 2005. First evidence for ultrahigh-pressure garnet peridotite in the North American Cordillera. Geology, 33, 105-108.

Milholland, C.S., Presnall, D.C., 1998. Liquidus phase relations in the CaO-MgO-Al_2O_3-SiO_2 system at 3.0 GPa: the aluminous pyroxene thermal divide and high-pressure fractionation of picritic and komatiitic magmas. Journal of Petrology, 39, 3-27.

Parkinson, C.D., Motoki, A., Onishi, C.E., Maruyama, S., 2001. Ultrahigh-pressure pyrope-kyanite granulites and associated eclogites in Neopreterozoic nappes of Southeast Brazil. UHPM Workshop 2001, Fluid/slab/mantle interactions and ultrahigh-P minerals. Waseda Univ., Tokyo, Abstract Volume, 87-90.

Pavese, A., Artioli, G., Russo, U., Hoser, A., 1999. Cation partitioning versus temperature in $(Mg_{0.70}Fe_{0.23})Al_{1.97}O_4$ synthetic spinel by in situ neutron powder diffraction. Physics and Chemistry of Minerals, 26, 242-250.

Pindell, J.L., Barrett, S.F., 1990. Geological evolution of the Caribbean region; a plate tectonic perspective. In: Dengo, G., Case, J.E. (eds.), The Caribbean Region: Boulder, Colorado, Geological Society of America, Geology of North America, H, 405-432.

Pindell, J., and Kennan, L., 2001. Kinematic evolution of the Gulf of Mexico and Caribbean. GCSSEMP Foundation 21st Annual Research Conference Transactions, Petroleum Systems of Deep-Water Basins, 193-220.

Pindell, J., and Kennan, L., 2009. Tectonic evolution of the Gulf of Mexico, Caribbean and northern South America in the mantle reference frame: an update. In: Lorente, J.K., and Pindell, J., eds., The Geology and Evolution of the region between North and South America: Geological Society of London, Special Publication, 328, 1-55.

Pindell, J., Kennan, L., Maresch, W.V., Stanek, K-P, Draper, G., Higgs, R., 2005. Plate-kinematics and crustal dynamics of circum-Caribbean arc-continent interactions and tectonic controls on basin development. In: Avé Lallemant, H. G., Sissons V. B. (eds.), Proto-Caribbean margins, in Caribbean - South American plate interactions, Venezuela. Geological Society of America Special Paper 394, 7-52, doi 10.1130/2005.2394(01).

Pindell, J., Maresch, W.V., Martens, U., Stanek, K., 2012. The Greater Antillean Arc: Early Cretaceous origin and proposed relationship to Central American subduction mélanges: implications for models of Caribbean evolution. International Geology Review, 54, 131-143.

Powell, R., 2005. THERMOCALC, (v. tc325) web site: www.metamorph.geo.uni-mainz.de /thermocal/.

Powell, R., Holland, T.J.B., Worley, B.A., 1998. Calculating phase diagrams involving solutions via on-linear equations, with examples using THERMOCALC. Journal of Metamorphic Geology, 16, 577-588.

Roselle, G.T., Thuring, M., Engi, M., 2002. MELONPIT: A finite element code for simulating tectonics mass movement and heat flow within subduction zones. American Journal of Science, 302, 381-409.

Sack, R.O., Ghiorso, M.S., 1994. Thermodynamics of multicomponent pyroxenes; I. Formulation of a general model. Contributions to Mineralogy and Petrology, 116, 277-286.

Smyth, J.R., 1980. Cation vacancies in the crystal chemistry of breakdown reactions in kimberlitic omphacites. American Mineralogist, 65, 1185-1191.

Spear, F.S., 1993. Metamorphic Phase Equilibria and Pressure-Temperature-Time Paths. Mineralogical Society of America, Monograph Series, 799 p.

Stanek, K.P., Maresch, W.V., Pindell, J.L., 2009. The geotectonic story of the northwestern branch of the Caribbean Arc: Implications from structural and geochronological data of Cuba. In: James, K.H., Lorente, M.A., Pindell, J.L., eds., The Origin and Evolution of the Caribbean Plate. Geological Society, London, Special Publications, 328, 361-398.

Sun, S., McDonough, W.F., 1989. Chemical and isotopic systematics of oceanic basalts: Implications for mantle composition and processes. In: Saunders, A.D., Norry, M.J. (eds.), Magmatism in ocean basins. Blackwell Scientific, Boston, 313-345.

Till, A.B., 1981. Alpine-type garnet lherzolite of the Kigluaik Mountains, Seward Peninsula, Alaska. Geological Society of America Abstracts with Programs, 13(2), 110.

Walter, M.J., 1998. Melting of garnet peridotite and the origin of komatiite and depleted lithosphere. Journal of Petrology, 39, 29-60.

Wei, C.J., Clarke, G.L., 2011. Calculated phase equilibria for MORB compositions: a reappraisal of the metamorphic evolution of lawsonite eclogite. Journal of Metamorphic Geology, 29, 939-952.

Whitney, D.L., Evans, B.W., 2010. Abbreviations for names of rock-forming minerals. American Mineralogist. 95, 185-187.

Manuscript received June 2011;
revision accepted October 2012;
published Online November 2012.

ELECTRONIC APPENDIX

Geochemistry of Eclogite

Two samples of the retrograded eclogite were selected for preliminary whole rock chemical analyses. The results are reported in Table A1 and Figure A1. Both samples are described in detail in Abbott and Draper (2007). Sample DR05-6 (unit Kc2) represents, both modally and texturally, the typical eclogite, differing little from DR05-2, discussed in this paper (Fig. 8). Also as discussed in this paper (and see Fig. 9, Table 2), sample DR00-6 (unit Kc3) is unusual for the development of two types of symplectite (Sym-I and Sym-II). The major element chemistry of both samples is consistent with low-K tholeiitic basalt in the IUGS classification system. DR05-6 is quartz-normative; whereas, DR00-6 is olivine-normative. Figure A1 shows the rare earth elements, normalized to MORB (Sun and McDonough, 1989). Ratios for DR05-6 are all close to unity; hence, DR05-6 faithfully preserves the signature of an MORB provenance (Sun and McDonough, 1989), despite a protracted metamorphic history. The data are consistent with the MORB-group in a more comprehensive trace-element data-set for rock samples from the same unit (Kc2) (Escuder-Viruete, 2009). Except for the strong positive Eu-anomaly, the REE pattern for DR00-6 (unit Kc3) mimics the pattern for DR05-6 but with systematically lower REE ratios. The strong positive Eu-anomaly suggests that DR00-6 was a plagioclase cumulate. The pattern can be modeled reasonably well as ~75% cumulate plagioclase and ~25% melt of the composition of N-MORB or DR05-6. The unpublished data (Escuder-Viruete, 2009) also indicates an island-arc tholeiite (IAT) component in all three units of the Cuaba gneiss. While in some respects the REE pattern for sample DR00-6 resembles the REE patterns for the IAT component, none of the latter show Eu anomalies. Also, low Th and very high Pb values for sample DR00-6 contrast strongly with the high Th and low Pb values in rocks with the IAT signature.

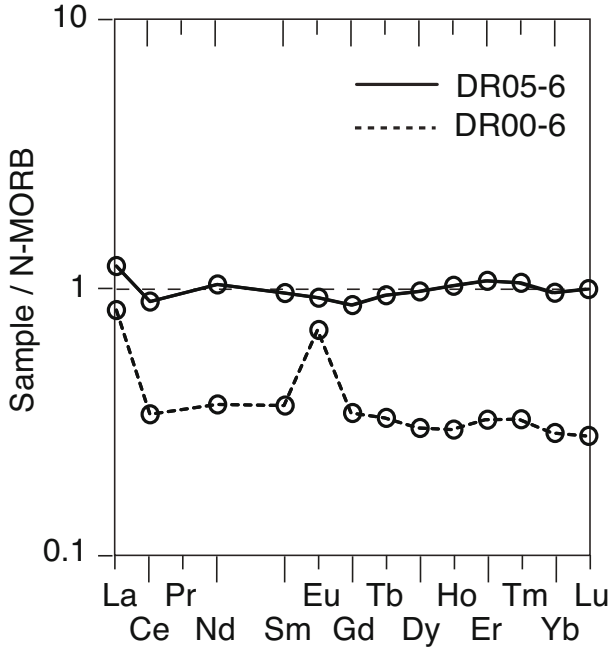

FIGURE I | REE analyses for eclogite samples DR05-6 and DR00-6, normalized to N-MORB (Sun and McDonough, 1989).

TABLE I | Bulk rock chemistry[1], Eclogite

	DR05-6	DR00-6
	wt%	
SiO_2	51.62	45.17
Al_2O_3	15.01	17.07
Fe_2O_3(T)	12.06	16.82
MnO	0.184	0.256
MgO	6.56	5.79
CaO	10.54	10.99
Na_2O	2.78	2.32
K_2O	0.06	0.03
TiO_2	1.404	1.316
P_2O_5	0.11	0.01
LOI	0.17	0.04
Total	100.5	99.81
	ppm	
Sc	39	50
Be	1	2
V	304	634
Cr	200	< 20
Co	36	50
Ni	70	< 20
Cu	10	100
Zn	50	120
Ga	16	21
Ge	1.4	1.5
As	< 5	< 5
Rb	2	< 1
Sr	113	377
Y	27.8	7.6
Zr	60	7
Nb	1.1	0.5
Mo	< 2	< 2
Ag	< 0.5	< 0.5
In	< 0.1	< 0.1
Sn	< 1	< 1
Sb	0.4	1.6
Cs	< 0.1	0.1
Ba	33	27
La	3.02	2.07
Ce	6.68	2.54
Pr	1.34	0.45
Nd	7.53	2.69
Sm	2.52	0.96
Eu	0.939	0.712
Gd	3.18	1.26
Tb	0.63	0.22
Dy	4.42	1.37
Ho	1.03	0.3
Er	3.16	0.96
Tm	0.477	0.148
Yb	2.93	0.88
Lu	0.451	0.128
Hf	1.8	0.3
Ta	< 0.01	< 0.01
W	0.8	3
Tl	< 0.05	< 0.05
Pb	< 5	9
Bi	< 0.1	< 0.1
Th	0.18	< 0.05
U	0.12	0.04

[1]Method: Oxide species, LOI, Sc, Be, V, Sr, Ba by fused glass bead, ICP. All other species by fused glass bead, MS. Activation Laboratories, Ltd., Canada. (June 2009)